Acta Crystallographica Section B
Structural Science
ISSN 0108-7681

Evidence for differentiation in the iron-helicoidal chain in $GdFe_3(BO_3)_4$

S. A. Klimin,[a,b] D. Fausti,[a]* A. Meetsma,[a] L. N. Bezmaternykh,[c] P. H. M. van Loosdrecht[a] and T. T. M. Palstra[a]

[a]Material Science Center, University of Groningen, 9747 AG Groningen, The Netherlands, [b]Institute of Spectroscopy, RAS, 142190, Troitsk, Moscow Region, Russian Federation, and [c]L. V. Kirensky Institute of Physics, Siberian Branch of RAS, Krasnoyarsk 660036, Russian Federation

Correspondence e-mail: d.fausti@rug.nl

Received 15 February 2005
Accepted 1 June 2005

A single-crystal X-ray structure study of gadolinium triiron tetraborate, $GdFe_3(BO_3)_4$, at room temperature and at 90 K is reported. At room temperature $GdFe_3(BO_3)_4$ crystallizes in a trigonal space group, $R32$ (No. 155), the same as found for other members of the iron borate family $RFe_3(BO_3)_4$. At 90 K the structure of $GdFe_3(BO_3)_4$ transforms to the space group $P3_121$ (No. 152). The low-temperature structure determination gives new insight into the weakly first-order structural phase transition at 156 K and into the related Raman phonon anomalies. The presence of two inequivalent iron chains in the low-temperature structure provides a new perspective on the interpretation of the low-temperature magnetic properties.

1. Introduction

The family of borates $RM_3(BO_3)_4$, where R is a rare earth metal (RE) or yttrium, and M is Al, Ga, Fe or Sc, crystallize in the huntite, $CaMg_3(CO_3)_4$, structure type with space group $R32$ (Joubert *et al.*, 1968; Belokoneva *et al.*, 1979; Campá *et al.*, 1997). Interest in this family of crystals arises both from a fundamental point of view and from already realized and proposed applications. Crystals of $YAl_3(BO_3)_4$ and $GdAl_3(BO_3)_4$ doped with Nd have been widely studied during recent years and have been used in optical devices such as self-frequency doubling and self-frequency summing lasers (*e.g.* Brenier *et al.*, 2004, and references therein). Concentrated $NdAl_3(BO_3)_4$ crystals are efficient media for minilasers (Chen *et al.*, 2001).

Apart from the interesting optical properties arising chiefly from the lack of inversion symmetry, the 'sub-family' of $RFe_3(BO_3)_4$ compounds also attracts considerable attention as a result of their structural peculiarities. The presence of magnetic order at temperatures of less than 37 K was attributed to magnetic Fe—Fe or Fe—O—Fe interactions inside quasi-one-dimensional iron chains (Campá *et al.*, 1997; Balaev *et al.*, 2003). Recent work (Levitin *et al.*, 2004; Balaev *et al.*, 2003), focusing on low-temperature magnetism in $GdFe_3(BO_3)_4$, revealed two magnetic phase transitions. The second-order magnetic ordering phase transition at $T_{N1} = 37$ K (antiferromagnetic ordering of Fe atoms) is followed by a first-order spin-reorientational phase transition at $T_{N2} = 10$ K. Additionally, specific heat and Raman measurements on single crystals (Levitin *et al.*, 2004) of $GdFe_3(BO_3)_4$ revealed a weakly first-order structural phase transition at $T_s = 156$ K. This structural phase transition is observed in almost all members of the RE ferroborate family (Hinatsu *et al.*, 2003; Levitin *et al.*, 2004; Fausti *et al.*, 2005). Recently, Hinatsu *et al.* (2003), by measuring the temperature dependence of the lattice parameters on powder samples, have shown that $DyFe_3(BO_3)_4$ undergoes such a structural phase transition at

340 K. Here too a peak in the specific heat was observed at this temperature. Similar peaks in specific heat *versus* temperature dependence were found for other heavy RE ferroborates (R = Eu–Ho, Gd and Tb). These peaks were ascribed to structural phase transitions. The transition temperatures T_s were found to depend linearly on the ionic radius of the RE. To date, there are no single-crystal data available nor has the low-temperature (LT) space group been determined.

The high-temperature (HT) $R32$ structure of powder $RFe_3(BO_3)_4$ compounds was first determined by Joubert *et al.* (1968) for R = La, Nd, Sm–Ho and Y. X-ray experiments on single crystals with $R = Nd_{0.5}Bi_{0.5}$ (Belokoneva *et al.*, 1979) and R = La, Nd and $Y_{0.5}Bi_{0.5}$ (Campá *et al.*, 1997) confirmed this structure. Moreover, Raman measurements for $LaFe_3(BO_3)_4$ (De Andres *et al.*, 1997), $NdFe_3(BO_3)_4$ (De Andres *et al.*, 1997; Fausti *et al.*, 2005) and $GdFe_3(BO_3)_4$ (Fausti *et al.*, 2005) are in good agreement with group theoretical analysis, based on the $R32$ structure.

Summarizing, whereas the HT crystal structure of most of the ferroborates is known, the LT space group, lattice parameters and atomic positions are unknown. In this work we report a single-crystal X-ray diffraction structure study of gadolinium iron borate at room temperature (RT) and at 90 K. It is found that the LT structure has $P3_121$ symmetry. The fact that two nonequivalent spin chains exist in the LT structure gives new insight into the low-temperature magnetic properties. The $P3_121$ symmetry of the LT phase also confirms the interpretation of the reported IR absorption by crystal-field transitions (Levitin *et al.*, 2004; Chukalina *et al.*, 2004) and leads to a better understanding of some peculiarities observed in Raman spectra (Levitin *et al.*, 2004; Fausti *et al.*, 2005).

2. Experimental and results of structure determination

Crystals of $GdFe_3(BO_3)_4$ were grown using a $K_2Mo_3O_{10}$-based flux, as described by Balaev *et al.* (2003). The large transparent single crystals were light green in color and had a good optical quality. A block-shaped crystal ('broken fragment') with dimensions 0.22 × 0.15 × 0.11 mm was mounted on top of a glass fiber and aligned on a Bruker SMART APEX CCD diffractometer. The crystal was cooled to 90 (1) K using a Bruker Kryoflex device. Intensity measurements were performed using graphite-monochromated Mo $K\alpha$ radiation. Generator settings were 50 kV/40 mA. *SMART* (Bruker, 2000) was used for preliminary determination of the unit-cell parameters and data collection control. The intensities of reflections of a hemisphere were collected by a combination of six sets of exposures (frames). Each set had a different angle for the crystal and each exposure covered a range of 0.3° in ω. A total of 3600 frames were collected with an exposure time of 10.0 s per frame. The overall data collection time was 16 h. Data integration and global cell refinement was performed with the program *SAINT* (Bruker, 2000). The final unit cell was obtained from the *xyz* centroids of 4767 and 5439 reflections after integration for the RT and 90 K structures, respectively. Intensity data were corrected for Lorentz and polarization effects, scale variation, decay and absorption (an analytical absorption correction was applied), and reduced to F_o^2. The program suite *SHELXTL* was used for space-group determination (*XPREP*; Bruker, 2000).

At both temperatures the unit cell was identified as trigonal; reduced cell calculations did not indicate any higher metric lattice symmetry (Spek, 1988). Space groups $R32$ and $P3_121$ were derived for the RT and 90 K structures, respectively, from the systematic extinctions and were discriminated from other candidate space groups that comply with the same extinctions conditions during the structure determination process. Examination of the final atomic coordinates of the structure did not yield extra crystallographic or metric symmetry elements (Le Page, 1987, 1988). The polarity of the structure of the crystal actually chosen was determined by Flack's **x** refinement

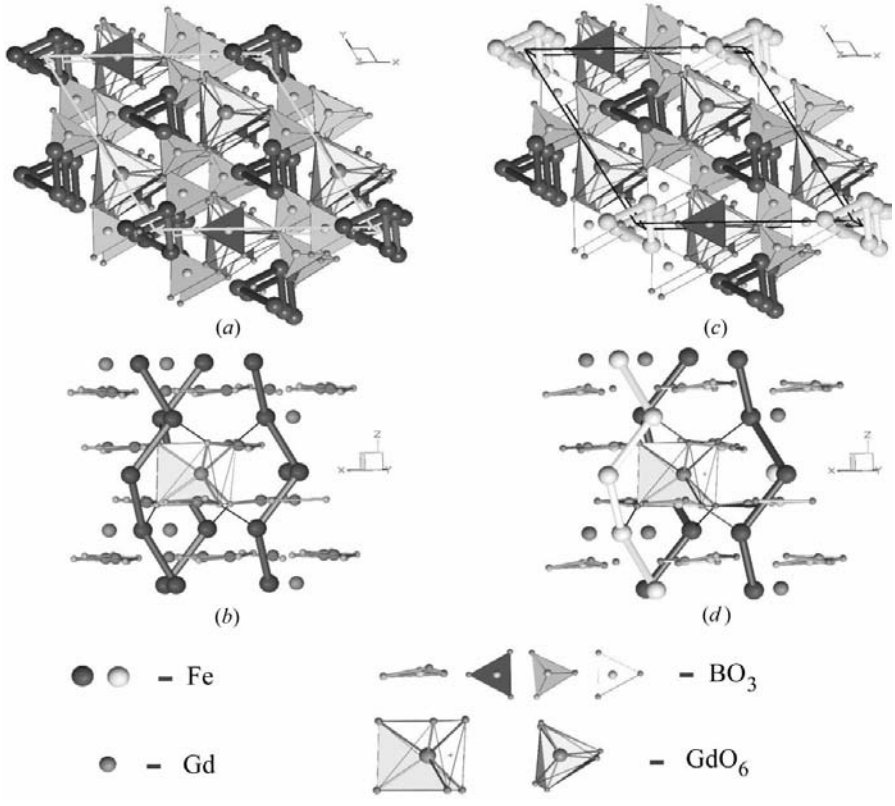

Figure 1
The structure of $GdFe_3(BO_3)_4$ in two different projections. The left panels, (*a*) and (*b*), show the RT structure, and the right panels, (*c*) and (*d*), show the structure at 90 K. The Fe atoms are arranged in chiral chains parallel to the *c* axis. Different chains are separated by GdO_6 prisms and BO_3 groups. The unit-cell outline for $R32$ is shifted by ($\frac{1}{3}$, $\frac{1}{3}$, 0) for comparison with the LT $P3_121$ structure.

Table 1
Experimental details.

	LT	RT
Crystal data		
Chemical formula	$GdFe_3(BO_3)_4$	$GdFe_3(BO_3)_4$
M_r	560.04	560.04
Cell setting, space group	Trigonal, $P3_121$	Trigonal, $R32$
a, b, c (Å)	9.5305 (3), 9.5305 (3), 7.5479 (2)	9.5203 (6), 9.5203 (6), 7.5439 (5)
V (Å^3)	593.73 (3)	592.15 (7)
Z	3	3
D_x (Mg m^{-3})	4.699	4.712
Radiation type	Mo $K\alpha$	Mo $K\alpha$
No. of reflections for cell parameters	5439	4767
θ range (°)	3.7–38.5	3.7–38.7
μ (mm^{-1})	13.74	13.77
Temperature (K)	90 (1)	297 (1)
Crystal form, color	Broken block, light green	Broken block, light green
Crystal size (mm)	0.22 × 0.15 × 0.11	0.22 × 0.15 × 0.11
Data collection		
Diffractometer	Bruker SMART APEX	Bruker SMART APEX
Data collection method	φ and ω scans	φ and ω scans
Absorption correction	Analytical	Analytical
T_{min}	0.062	0.056
T_{max}	0.251	0.252
No. of measured, independent and observed parameters	13 868, 2217, 1956	4700, 755, 755
Criterion for observed reflections	$I > 2\sigma(I)$	$I > 2\sigma(I)$
R_{int}	0.034	0.034
θ_{max} (°)	38.6	38.7
Range of h, k, l	$-16 \Rightarrow h \Rightarrow 16$ $-16 \Rightarrow k \Rightarrow 16$ $-13 \Rightarrow l \Rightarrow 13$	$-16 \Rightarrow h \Rightarrow 16$ $-16 \Rightarrow k \Rightarrow 16$ $-13 \Rightarrow l \Rightarrow 13$
Refinement		
Refinement on	F^2	F^2
$R[F^2 > 2\sigma(F^2)]$, $wR(F^2)$, S	0.017, 0.045, 0.86	0.015, 0.037, 1.07
No. of reflections	2217 reflections	755 reflections
No. of parameters	95	35
H-atom treatment	No H atoms present	No H atoms present
Weighting scheme	$w = 1/[\sigma^2(F_o^2) + (0.0312P)^2 + 0.P]$ where $P = (F_o^2 + 2F_c^2)/3$	$w = 1/[\sigma^2(F_o^2) + (0.0272P)^2 + 0.P]$ where $P = (F_o^2 + 2F_c^2)/3$
$(\Delta/\sigma)_{max}$	0.003	<0.0001
$\Delta\rho_{max}$, $\Delta\rho_{min}$ (e Å^{-3})	0.82, −0.51	0.62, −0.97
Extinction method	*SHELXL*	*SHELXL*
Extinction coefficient	0.0359 (10)	0.0371 (12)
Absolute structure	Enantiomorph twin refinement resulted in 0.50 (1) so ultimately set to 0.5 (Flack & Bernardinelli, 1999, 2000)	Enantiomorph twin refinement resulted in 0.50 (1) so ultimately set to 0.5 (Flack & Bernardinelli, 1999, 2000)
Flack parameter	0.5	0.5

† Computer programs used: *SMART* (Version 5.624; Bruker, 2000), *SAINT* (Version 6.02A; Bruker, 2000), *XPREP* (Version 5.1/NT; Bruker, 2000), *SIR97* (Altomare *et al.*, 1999), *SHELXL97* (Sheldrick, 1997), *PLUTO* (Meetsma, 2003), *ORTEP* (Farrugia, 1997), *PLATON* (Spek, 1994, 2003).

(Flack, 1983; Flack & Bernardinelli, 1999, 2000; Herbst-Irmer & Sheldrick, 1998); refinement resulted in an **x** value of 0.50 (1), so ultimately an inversion twin was used in the refinement.

Crystal data and numerical details on data collection and refinement are given in Table 1.[1]

3. Discussion of the structure

After a brief introduction describing the main features of $GdFe_3(BO_3)_4$, we will focus on the difference between the RT and the 90 K (LT) structures. Firstly, we will try to understand the consequences that the structural changes have on the interpretation of Raman spectra anomalies at the weak first-order phase transition reported in the literature (Levitin *et al.*, 2004). Secondly, we will give a new perspective for the interpretation of low-temperature magnetic data (Levitin *et al.*, 2004; Balaev *et al.*, 2003).

The RT structure of $GdFe_3(BO_3)_4$ belongs to the $R32$ space group (Figs. 1*a* and 1*b*). Our measurement confirms the structure reported previously for powder samples (Joubert *et al.*, 1968) and for several single crystals (Belokoneva *et al.*, 1979; Campá *et al.*, 1997) from the family $RFe_3(BO_3)_4$. The structure consists of alternating layers (parallel to the *ab* plane) of FeGd and BO_3 groups (see Fig. 1*b*). The main features of this structure have already been described by Campá *et al.* (1997); the BO_3 groups are arranged in layers nearly perpendicular to the C_3 axis and the Fe atoms are arranged in helicoidal chains parallel to this axis. Different chains are connected by GdO_6 and BO_3 groups, where each individual BO_3 and GdO_6 group connects three chains. The distance between Fe atoms in the same chain [3.1669 (4) Å] is shorter than the shortest distance, 4.8308 (5) Å, between Fe atoms in different chains. The main exchange interaction between Fe^{3+} ions is therefore of a quasi-one-dimensional nature.

Upon lowering the temperature, the symmetry of the $GdFe_3(BO_3)_4$ crystal reduces from $R32$ to $P3_121$, in the trigonal system. Fig. 2 shows the coordination polyhedra (GdO_6, FeO_6 and BO_3) for the two different structures. At RT the BO_3 groups occupy two inequivalent positions, B1 (D_3) and B2 (C_2). At 90 K the site symmetry of the B1 atoms is reduced to C_2, whereas the site symmetry of the B2 atoms differentiates into B2*b* (C_2) and B2*a* (C_1) (see also Table 2). In the LT phase, the angle between the BO_3 groups and the *c* axis is changed. Moreover, in the LT phase, the BO_3 groups in the C_1 position are considerably distorted and no longer flat (see Table 2).

The LT structure is in agreement with the Raman data (Levitin *et al.*, 2004; Fausti *et al.*, 2005). The group theoretical vibrational analysis, based on the 90 K structure, shows that, as a result of the lowering of the symmetry, new librational modes of the BO_3 group become Raman active (R_x and R_y). The observed structural change is compatible with an appearance of the librational R_y mode of the BO_3 group upon approaching T_s from above, and a subsequent hardening of this mode in the LT phase (see Fig. 3). Also the anisotropic

[1] Supplementary data for this paper are available from the IUCr electronic archives (Reference: LC5026). Services for accessing these data are described at the back of the journal.

displacement parameters U_{33} of the O atoms suggest that the borate groups are relatively free to oscillate around the *y* axis.

Concerning the magnetic structure, the main peculiarity of both the RT and the 90 K structures is the existence of magnetically quasi-one-dimensional helicoidal iron chains (see Fig. 1). The intrachain exchange interaction between the Fe ions is expected to be dominated by Fe—Fe direct exchange and Fe—O—Fe superexchange, depending, respectively, on the Fe—Fe distance and two Fe—O—Fe angles (Fig. 4). Nevertheless there are some significant differences.

At RT all the Fe atoms are in equivalent positions (C_2). All Fe chains are equivalent, as are the Fe—O—Fe angles [102.40 (12) and 103.65 (8)°] and Fe—Fe distances [3.1669 (4) Å]. Therefore, the exchange interactions between neighboring iron ions within a chain are also equivalent. At LT (Fig. 1), as shown in Table 2, the BO_3 groups form one general triangle (gray, C_1 position) and two isosceles triangles (white

Table 2
Symmetry positions of BO_3 groups, angles between the groups and the *c* axis, and the flatness of the BO_3 groups.

The flatness is expressed as the distance of the B atoms from the plane defined by the three oxygen ligands.

Room temperature				Low temperature			
	Symmetry	Angle (°)	Flatness (Å)		Symmetry	Angle (°)	Flatness (Å)
B1	D_3	90	0	B1	C_2	87.52(4)	0.00002 (4)
B2	C_2	84.37 (11)	0	B2*a*	C_1	81.89	0.0055 (11)
				B2*b*	C_2	83.55	0.0000 (2)

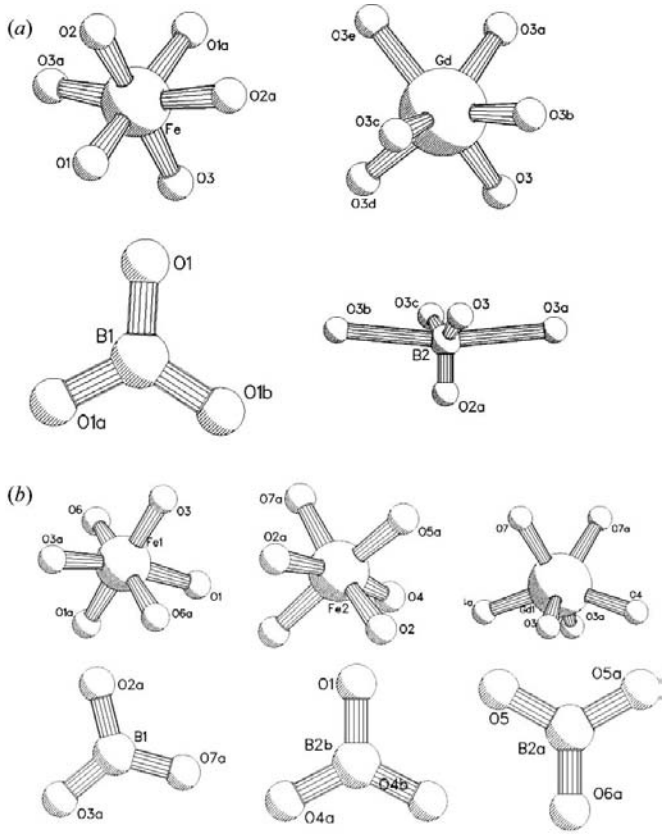

Figure 2
Coordination polyhedra for the RT [*R*32-(*a*)] and the LT [$P3_121$-(*b*)] structures of $GdFe_3(BO_3)_4$. At RT the Fe atoms with C_2 symmetry are coordinated by three different types of O atoms. At 90 K there are two inequivalent positions for the Fe atoms: Fe1 (the same symmetry as RT) and Fe2, which is in a general position (surrounded by five different types of O atom). At RT the Gd atoms are surrounded by six O atoms of one type (D_3 symmetry). At 90 K the Gd atoms are coordinated by three different types of O atom (C_2 symmetry). For the B atoms there are two kinds of coordination at RT. Atom B1 (in D_3 symmetry) is surrounded by three O atoms of the same type; the $B1O_3$ group is thus an equilateral triangle. The B2 atoms are surrounded by two types of O atom; $B2O_3$ is an isosceles triangle (C_2 symmetry). At 90 K there are three kinds of coordinations for the B atoms; $B2bO_3$ and $B1O_3$ are isosceles triangles (C_2symmetry) and $B2aO_3$ is general triangle.

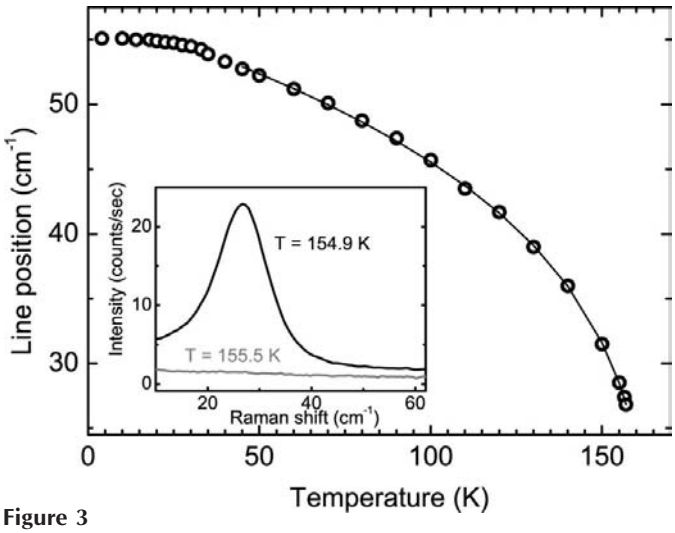

Figure 3
Temperature dependence of Raman frequency of the low-energy mode appearing at the structural phase transition T_s. Insert shows the low-frequency part of the Raman spectrum at two close temperatures, before and after phase transition.

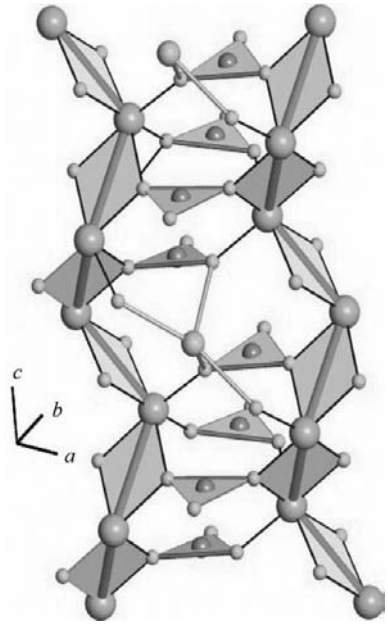

Figure 4
Two Fe chains and the most important exchange paths; the intrachain exchange is *via* Fe—Fe direct exchange or Fe—O—Fe superexchange, while the interchain exchange is through Fe—O—Gd—O—Fe and Fe—O—O—Fe.

and dark, C_2 position). At RT 'gray' and 'white' groups also become equivalent, with C_2 symmetry, and the 'dark' group is a regular triangle with D_3 symmetry. The reduction of the symmetry of the borate groups changes the environment of the Fe atoms (Fig. 2), yielding two inequivalent positions (C_2 and C_1). Therefore, the Fe—Fe distances are different for the two chains: one is stretched [3.1828 (4) Å] and in the other is compressed [3.1554 (4) Å]. The Fe—O—Fe angles for the first chain are 101.24 (5) and 103.71 (9)°, while those for the second are 102.46 (6) and 103.91 (8)°. Therefore, the intrachain exchange interaction is also different for the two chains.

The GdO_6 prism connects three chains: one containing Fe1 atoms with C_2 symmetry and two with Fe2 atoms in general positions. There is only one inequivalent position for the Gd atoms in each of the RT and the 90 K structures. However, the site symmetry of the Gd atoms changes from D_3 at RT to C_2 at 90 K. This fact confirms the conclusion of Levitin *et al.* (2004), who interpreted low-temperature IR spectra of $Nd_{0.01}Gd_{0.99}Fe_3(BO_3)_4$ in terms of Kramer's doublets of Nd, assuming only one structural position for the Nd ions.

The detailed structure of the Fe chains and their interconnection are shown in Fig. 4. The intrachain interactions between Fe atoms are *via* two Fe—O—Fe superexchange pathways. The magnetic interchain interaction arises from the Fe—O—O—Fe and possibly the Fe—O—Gd—O—Fe superexchange path. The role of the first superexchange path is important because the substitution of Gd for non-magnetic Y does not lead to a disappearance of three-dimensional magnetic ordering. On the contrary, the Néel temperature for $YFe_3(BO_3)_4$, T_{N1} = 40 K, is larger than that found for the Gd compound (T_{N1} = 37 K) and for $NdFe_3(BO_3)_4$ (T_{N1} = 30 K) (Chukalina *et al.*, 2004; Fausti *et al.*, 2005). Considering the different RE^{3+} ionic radii (0.983 Å for Nd, 0.938 Å for Gd and 0.900 Å for Y) it is clear that the Neél temperature of $RFe_3(BO_3)_4$ depends strongly on the ionic radii: a smaller ionic radius results in a higher T_{N1}. Moreover, T_{N1} does not seem to be affected by the spin of the RE. In this sense it is clear that the main superexchange path of the interaction between different chains is the Fe—O—O—Fe path, and that a small distortion of this path changes substantially the magnetic properties of the system. It is therefore clear that the existence of two nonequivalent Fe chains with different Fe—Fe distances and Fe—O—Fe angles could lead to substantially different intrachain exchange constants for the two chains (Goodenough, 1955), and this fact should be taken into account for the interpretation of the magnetic properties.

4. Conclusions

In summary, we have determined the crystal structure of $GdFe_3(BO_3)_4$ at RT and 90 K. At RT $GdFe_3(BO_3)_4$ exhibits an *R*32 structure, in agreement with the results of Joubert *et al.* (1968) and Campá *et al.* (1997). Below the structural phase transition (T_s = 156 K) the structure has the $P3_121$ space group. The main difference between the LT and RT structures is the lowering of the symmetry and the tilt of the BO_3 groups. This difference confirms the interpretation of the Raman spectra of this phase transition. The main conclusion resulting from the LT structure determination is the presence of two inequivalent positions for the Fe atoms, giving rise to two different iron helicoidal chains.

The authors are very grateful to M. N. Popova for valuable discussions. This work was partially supported by the Stichting voor Fundamenteel Onderzoek der Materie [FOM, financially supported by the Nederlandse Organisatie voor Wetenschappelijk Onderzoek (NWO)]. SAK acknowledges the support of the Russian Foundation for Basic Research, grant [1]04-02-17346, and the Russian Academy of Sciences under the Programs for Basic Research.

References

Altomare, A., Burla, M. C., Camalli, M., Cascarano, G. L., Giacovazzo, C., Guagliardi, A., Moliterni, A. G. G., Polidori, G. & Spagna, R. (1999). *J. Appl. Cryst.* **32**, 115–119.
Balaev, A. D., Bezmaternykh, L. N., Gudim, I. A., Temerov, V. L., Ovchinnikov, S. G. & Kharlamova, S. A. (2003). *J. Magn. Magn. Mater.* **532**, 258–259.
Belokoneva, E. L., Alshinskaya, L. I., Simonow, M. A., Leonyuk, N. I., Timchenko, T. I. & Belov, N. B. (1979). *Zh. Strukt. Khim.* (*Russ. J. Struct. Chem.*), **20**, 542–544.
Brenier, A., Tu, C., Zhu, Z. & Wu, B. (2004). *Appl. Phys. Lett.* **84**, 2034–2036.
Bruker (2000). *SMART*, *SAINT*, *SADABS*, *XPREP* and *SHELXTL/NT*. Bruker AXS Inc., Madison, Wisconsin, USA.
Campá, J., Cascales, C., Gutierrez-Puebla, E., Monge, M., Rasines, I. & Ruiz-Valero, C. (1997). *Chem Mater.* **9**, 237–240.
Chen, X., Luo, Z. & Jaque, D. (2001). *J. Phys. Condens. Matter*, **13**, 1171–1178.
Chukalina, E. P., Kuritsin, D. Y., Popova, M. N., Bezmaternykh, L. N., Kharlamova, S. A. & Temerov, V. L. (2004). *Phys. Lett. A*, **322**, 239–243.
De Andres, A., Agullo-Rueda, F., Taboada, S., Cascales, C., Camp, J., Ruiz-Valero, C. & Rasines, I. (1997). *J. Alloys Compd.* **250**, 396–399.
Farrugia, L. J. (1997). *J. Appl. Cryst.* **30**, 565.
Fausti, D., Klimin, S. A. & van Loosdrecht, P. H. M. (2005). Unpublished.
Flack, H. D. (1983). *Acta Cryst.* A**39**, 876–881.
Flack, H. D. & Bernardinelli, G. (1999). *Acta Cryst.* A**55**, 908–915.
Flack, H. D. & Bernardinelli, G. (2000). *J. Appl. Cryst.* **33**, 1143–1148.
Goodenough, J. B. (1955). *Phys. Rev.* **100**, 564–573.
Herbst-Irmer, R. & Sheldrick, G. M. (1998). *Acta Cryst.* B**54**, 443–449.
Hinatsu, Y., Doi, Y., Ito, K., Wakeshima, M. & Alemi, A. (2003). *J. Solid State Chem.* **172**, 438–445.
Joubert, J. C., White, W. & Roy, R. (1968). *J. Appl. Cryst.* **1**, 318–319.
Le Page, Y. (1987). *J. Appl. Cryst.* **20**, 264–269.
Le Page, Y. (1988). *J. Appl. Cryst.* **21**, 983–984.
Levitin, R. Z., Popova, E. A., Chtsherbov, R. M., Vasiliev, A. N., Popova, M. N., Chukalina, E. P., Klimin, S. A., van Loosdrecht, P. H. M., Fausti, D. & Bezmaternykh, L. N. (2004). *JETP Lett.* **79**, 423–426.
Meetsma, A. (2003). Extended version of the program *PLUTO*. Groningen University, The Netherlands. (Unpublished.)
Sheldrick, G. M. (1997). *SHELXL97*. University of Göttingen, Germany.
Spek, A. L. (1988). *J. Appl. Cryst.* **21**, 578–579.
Spek, A. L. (1994). *Am. Crystallogr. Assoc. Abstr.* **22**, 66.
Spek, A. L. (2003). *J. Appl. Cryst.* **36**, 7–13.